



Luo, J., Jiang, J. Z., & Macdonald, J. (2019). Cable Vibration Suppression with Inerter-based Absorbers. *Journal of Engineering Mechanics*, 145(2), [04018134].
[https://doi.org/10.1061/\(ASCE\)EM.1943-7889.0001554](https://doi.org/10.1061/(ASCE)EM.1943-7889.0001554)

Peer reviewed version

License (if available):
Other

Link to published version (if available):
[10.1061/\(ASCE\)EM.1943-7889.0001554](https://doi.org/10.1061/(ASCE)EM.1943-7889.0001554)

[Link to publication record in Explore Bristol Research](#)
PDF-document

This is the accepted author manuscript (AAM). The final published version (version of record) is available online via ASCE at [https://doi.org/10.1061/\(ASCE\)EM.1943-7889.0001554](https://doi.org/10.1061/(ASCE)EM.1943-7889.0001554) . Please refer to any applicable terms of use of the publisher.

University of Bristol - Explore Bristol Research

General rights

This document is made available in accordance with publisher policies. Please cite only the published version using the reference above. Full terms of use are available:
<http://www.bristol.ac.uk/red/research-policy/pure/user-guides/ebr-terms/>

Cable Vibration Suppression with Inerter-based Absorbers

Jiannan Luo¹, Jason Zheng Jiang², and John H.G. Macdonald³

¹Department of Mechanical Engineering, University of Bristol, Bristol, BS8 1TR, UK.

²Department of Mechanical Engineering, University of Bristol, Bristol, BS8 1TR, UK.

(corresponding author). Email: z.jiang@bristol.ac.uk

³Department of Civil Engineering, University of Bristol, Bristol, BS8 1TR, UK.

ABSTRACT

Stay cables are prone to vibrations due to their low inherent damping. This paper presents an approach for systematic identification of beneficial passive absorbers layouts consisting of damper, spring and inerter. The inerter is a one-port mechanical element with the property that the applied force is proportional to the relative acceleration between its terminals. In this work, a finite element taut cable model, with vibration absorber represented by its admittance function, is firstly established. Two performance measures, depending on the length of the cable and the forcing conditions, are introduced to assess the effect of candidate absorbers. Potential advantages of low-complexity inerter-based absorber layouts are then systematically investigated, with corresponding element values in these layouts identified. Building on this, the effect of series compliance is also examined for beneficial absorber layouts. It is shown that, up to a certain inertance, which depends on the stiffness of the series compliance, the performance advantages over a viscous damper can be maintained, or even enlarged in some cases, if the element values are properly tuned.

INTRODUCTION

Stay cables are widely used in cable-stayed bridges and other civil engineering structures in order to carry static loads, but they are often observed to experience large amplitude vibrations. The exact excitation mechanisms are rather complex, but possible causes include aerodynamic forcing

on the cables such as galloping (Den Hartog 1933; Macdonald and Larose 2006), wake galloping (Tokoroa et al. 2000), rain–wind excitation (Hikami and Shiraishi 1988; Matsumoto et al. 1990) and excitation from deck or pylon motion (Lilien and Da Costa 1994; Macdonald 2016). However, large cable vibrations are more often caused by aerodynamic forcing which introduces aero-elastic instabilities. The motion of the cable in the wind causes changes in the aerodynamic forces which is often taken to be equivalent to negative damping. The classical instance of this is across-wind galloping (Den Hartog 1933), which often affects electricity transmission lines, especially with ice accretion. More generally, galloping can occur in a three-dimensional environment, such as for inclined bridge cables in skew wind (Macdonald and Larose 2006). When the negative aerodynamic damping is greater in magnitude than the structural damping, the vibrations grow exponentially (until nonlinearity may limit the amplitude at some large value). Other than changing the aerodynamic shape, which is not always possible or economic, the solution to galloping is to provide sufficient structural damping. For rain-wind excitation (Hikami and Shiraishi 1988; Matsumoto et al. 1990), which is the most common cause of large cable vibrations on cable-stayed bridges, it is generally considered also to be equivalent to some form of negative aerodynamic damping and it has been found to be inhibited by providing a certain level of damping (Caetano 2007). As a result, for limiting vibrations due to aerodynamic forcing on the cables, the damping ratio is often considered as the key parameter.

Adding viscous dampers to cables is a commonly-used method for introducing extra damping. Several studies have been carried out to understand the dynamic behavior. A universal curve have been presented for estimating the modal damping of stay cables with a viscous damper close to one of the supports (Pacheco et al. 1993), then an analytical formula for the universal curve was derived based on complex cable modes (Krenk 2000). Subsequently, Main and Jones extended these studies by revealing the importance of damper-induced frequency shifts in characterizing the response of the system (Main and Jones 2002). It has been shown that, the optimum damping ratio for a certain mode will be larger if the damper is located closer to an anti-node. However, for ease of installation and maintenance, they are usually located close to the deck end of the cable, up

51 to about 5% of the length along the cable (Cu and Han 2015). Tuned mass dampers (TMDs) are
52 another type of passive absorber device that has been used in practice on cables. It has been shown
53 that TMDs can be more effective than viscous dampers if they are fixed at the same location along
54 the cable (Cai et al. 2006).

55 An alternative is to use a vibration suppression device incorporating an inerter. The inerter
56 was proposed as an ideal two terminal mechanical element (Smith 2002), with the property that
57 the applied force is proportional to the relative acceleration between its two terminals. The inerter
58 has fundamentally enlarged the range of absorbers that can be realized mechanically. Furthermore,
59 via gearing, the inertance (i.e. the constant of proportionality between the relative acceleration
60 and force, with dimensions of mass) can be much larger than the physical mass of the device.
61 Performance advantages have been identified for road vehicles (Smith and Wang 2004; Jiang et al.
62 2015a), railway vehicles (Wang et al. 2009; Wang et al. 2012; Jiang et al. 2015b), aircraft landing
63 gear systems (Liu et al. 2015; Li et al. 2017a; Li et al. 2017b), and civil engineering structures
64 (Ikago et al. 2012; Lazar et al. 2014; Yang 2016; Zhang et al. 2017; Makris and Kampas 2016;
65 Bakis et al. 2017). For vibration suppression of cables, the potential benefits of adding a tuned
66 inerter damper (TID) system has been analyzed (Lazar et al. 2016). A practical tuning methodology
67 for the TID was proposed to minimize the displacement amplitude at the mid-span of the cable
68 for excitation from motion of both supports. However, cable vibrations caused by aerodynamic
69 forcing on the cables, which is usually more problematic have not been considered for inerter-based
70 absorbers.

71 Two performance measures are introduced in this paper to quantify the damping performance
72 of the absorbers. As the lowest frequency mode is often most susceptible to vibrations (Gimsing
73 and Georgakis 2011), one performance measure is the minimum damping ratio of any modes with
74 natural frequencies close to that of the first mode of the undamped cable, without considering
75 higher frequency modes. However, long cables or cables in extreme conditions may be susceptible
76 to vibrations in multiple modes, so the second measure takes higher modes into consideration. In
77 addition, the effects of series compliance to the absorber are introduced, since the connections at

78 either end of the absorber, to the support and to the cable, may not be fully rigid.

79 In this paper, the potential to enhance the damping performance of a cable, for passive absorber
80 layouts with three element or less is presented. The approach adopted enables candidate layouts,
81 i.e. specific connections of spring damper and inerter elements, to be explored in a systematic
82 manner. First, a finite element cable model is integrated with an admittance function representing a
83 general vibration absorber. All possible absorber layouts with no more than one damper, one inerter
84 and one spring each, as well as two proposed performance measures, are then introduced. After
85 that, the optimum performance of the modes with frequencies close to that of the first mode of the
86 undamped cable for all candidate layouts are identified, and the corresponding parameter values are
87 presented. Similar analysis, using the second measure to account for the effect on higher frequency
88 modes, is then implemented and results are presented. Finally, the effect of series compliance is
89 addressed for the two most beneficial layouts obtained in the previous section, before conclusions
90 are drawn.

91 **MATHEMATICAL APPROACH**

92 In this section, a finite element model of a cable combined with an arbitrary linear passive
93 absorber layout is introduced. Subsequently, all candidate absorber layouts with no more than one
94 damper, inerter and spring each are presented. Two performance measures are then introduced to
95 assess the damping performance. Following that, optimization results of a viscous damper only
96 layout is discussed and compared with previous studies, showing the validity of proposed approach.

97 **Cable models with admittance functions representing absorbers**

98 A mathematical model of a cable is built using the finite element method. Lumped masses rather
99 than bar elements are used here for the benefit of calculation efficiency, which will be discussed in
100 detail at the end of this subsection.

101 The tension along the cable is denoted as T , the total mass of the cable is M , and the total length
102 of the cable is L . The effects of inclination and sag of the cable are neglected as well as the cable's
103 out-of-plane motion and its elasticity. An example of a taut cable model with n DOF is shown in
104 Fig. 1. There are n masses, each of mass m spread along the cable and two masses of mass $m/2$

connected directly to the supports. Hence, $m = M/(n + 1)$. These masses divide the cable into $n + 1$ elements, each of length $l = L/(n + 1)$. The a^{th} mass has an associated vertical position x_a , which equals zero at equilibrium. Since the masses at the end-points are connected directly to the supports, x_0 and x_{n+1} always equal zero.

The displacement of the masses from their equilibrium positions leads to an angle θ_a between mass a and mass $a + 1$. As the displacements are small compared to the element length $L/(n + 1)$, the angle θ_a can be presented as:

$$\theta_a = \arcsin \left(\frac{x_{a+1} - x_a}{L/(n + 1)} \right) \quad (1)$$

The circular natural frequency of the first mode of the undamped cable model can be expressed as:

$$\omega_o = \pi \left(\frac{T}{ML} \right)^{0.5} \quad (2)$$

The equation of motion for mass a , without any external force, can be expressed as:

$$m\ddot{x}_a = T \sin(\theta_a) - T \sin(\theta_{a-1}) \quad (3a)$$

Similarly, the equation of motion for mass a_f , where the absorber is located, can be expressed as:

$$m\ddot{x}_{a_f} = T \sin(\theta_{a_f}) - T \sin(\theta_{a_f-1}) + F(t) \quad (3b)$$

where $F(t)$ is the force provided by the absorber. By substituting Eqs. (1) and (2) into Eqs. (3a) and (3b), Eqs. (4a) and (4b) can be obtained as below:

$$\frac{1}{n + 1} \ddot{x}_a = (n + 1) \cdot \left(\frac{\omega_o}{\pi} \right)^2 \cdot (x_{a+1} - 2x_a + x_{a-1}) \quad (4a)$$

$$\frac{1}{n + 1} \ddot{x}_{a_f} = (n + 1) \cdot \left(\frac{\omega_o}{\pi} \right)^2 \cdot (x_{a_f-1} - 2x_{a_f} + x_{a_f+1}) + \frac{F(t)}{M} \quad (4b)$$

Taking Laplace transforms of both sides of Eqs. (4a) and (4b), Eqs. (5a) and (5b) are obtained:

$$\frac{1}{n+1} s^2 \tilde{x}_a = (n+1) \cdot \left(\frac{\omega_o}{\pi}\right)^2 \cdot (\tilde{x}_{a-1} - 2\tilde{x}_a + \tilde{x}_{a+1}) \quad (5a)$$

$$\frac{1}{n+1} s^2 \tilde{x}_{a_f} = (n+1) \cdot \left(\frac{\omega_o}{\pi}\right)^2 \cdot (\tilde{x}_{a_f-1} - 2\tilde{x}_{a_f} + \tilde{x}_{a_f+1}) + \frac{Y(s)}{M} \cdot s \cdot \tilde{x}_{a_f}(s) \quad (5b)$$

where tildes indicate Laplace transforms and $Y(s) = \tilde{F}(s)/[s \cdot \tilde{x}_{a_f}(s)]$ represents the admittance function of the absorber, which is defined as the ratio of force to velocity.

It has been shown that all $Y(s)$ representing linear, passive absorbers are positive-real functions (Brune 1931). By arranging the displacement of each mass in the vector $\mathbf{x} = [x_1, x_2, x_3, \dots, x_n]^T$, Eqs. (5a) and (5b) can be rewritten in matrix form as:

$$\mathbf{M} s^2 \tilde{\mathbf{x}} + \mathbf{C} s \tilde{\mathbf{x}} + \mathbf{K} \tilde{\mathbf{x}} = \mathbf{0} \quad (6)$$

In Eq. (6), the elements of matrices \mathbf{M} , \mathbf{C} and \mathbf{K} are respectively described in Eqs. (7a)-(7c), in which δ_{ij} is the Kronecker delta function.

$$m_{ij} = \frac{1}{n+1} \delta_{ij} \quad (7a)$$

$$c_{ij} = 0, \text{ except } c_{a_f a_f} = -Y(s)/M \quad (7b)$$

$$k_{ij} = (n+1) \cdot \left(\frac{\omega_o}{\pi}\right)^2 \cdot (2\delta_{ij} - \delta_{i(j+1)} - \delta_{i(j-1)}) \quad (7c)$$

Complex eigenvalues of the system (represented by $[\lambda \quad \lambda^{*T}]^T$) are calculated as roots of Eq. (8), where $\lambda = [\lambda_1, \lambda_2, \lambda_3, \dots]$, $\mathbf{0}$ is the square null matrix of size n and \mathbf{I} is the identity matrix of size n .

$$\det \left(\begin{bmatrix} \mathbf{0} & \mathbf{I} \\ -\mathbf{M}^{-1} \mathbf{K} & -\mathbf{M}^{-1} \mathbf{C} \end{bmatrix} - \begin{bmatrix} s \mathbf{I} & \mathbf{0} \\ \mathbf{0} & s \mathbf{I} \end{bmatrix} \right) = 0 \quad (8)$$

It should be noted that \mathbf{C} is a function of s , so the eigenvalues of the system cannot be found by conventional numerical methods. However, Eq. (8) is still fundamentally valid, giving a polynomial

in s , the roots of which are the eigenvalues. By using a similar finite element model of a cable with a TID (Lazar et al. 2016), in which the internal DOFs of the TID was explicitly represented in the matrix equation of motion, making the vector \mathbf{x} $(n + 1)$ elements long and the matrices \mathbf{M} , \mathbf{C} and \mathbf{K} of size $(n + 1) \times (n + 1)$. Using that method, the matrices need to be reformulated for each alternative absorber layout. The advantage of the method presented here is that a system with any passive linear absorber can be represented by Eq. (6) and Eqs. (7a)-(7c), with \mathbf{x} always being n elements long and the matrices \mathbf{M} , \mathbf{C} and \mathbf{K} always of size $n \times n$. The only difference for different absorber layouts is the positive-real admittance function $Y(s)$ representing the absorber.

The roots of Eq. (8), i.e. $[\lambda \quad \lambda^{*T}]^T$, are in complex conjugate pairs. The number of pairs is given by n plus the number of internal DOFs of the absorber. However, normally only a few pairs, representing low frequency modes, are of interest. Either eigenvalue λ_e (with positive imaginary part, $e = 1, 2, 3, \dots$) or its complex conjugate eigenvalue λ_e^* can be used to calculate damping ratio ζ_e and circular natural frequency ω_e of mode e of the damped cable, which respectively are:

$$\zeta_e = -\text{Re}(\lambda_e) / \sqrt{\text{Re}(\lambda_e)^2 + \text{Im}(\lambda_e)^2} \quad (9a)$$

$$\omega_e = \sqrt{\text{Re}(\lambda_e)^2 + \text{Im}(\lambda_e)^2} \quad (9b)$$

The number of DOF of the cable, n , should be large enough to limit the error due to the finite element approximation. In order to balance accuracy and computational time, lumped masses rather than bar elements are used and a suitable number of DOF is selected. From preliminary analysis for a number of absorber layouts, it was typically found that a lumped mass model with 99 DOFs provides similar accuracy to a bar element model with 60 DOFs, but the bar element model took approximately twice the computational time. This is because the mass matrix for the bar element model is non-diagonal, which leads to a non-trivial inverse in Eq. (8). Hence for similar accuracy, the lumped mass model is more computationally efficient. The maximum relative difference in the damping ratio ζ_e between lumped mass models with 99 and 999 DOFs was found to be typically less than 0.1%, considering only low frequency modes with natural frequencies

below $6.5\omega_o$. Therefore, a 99 DOF lumped mass model is used for the analysis in the present study. Furthermore, since the present study is more focused on a systematic approach to identify beneficial absorber layouts, and also for a fair comparison, the location of all candidate absorbers in this study is set to be at 5% length of the whole cable.

Candidate absorber layouts and non-dimensionalized parameters

In previous study (Lazar et al. 2016), only one specific layout, namely a TID structure is considered. Taking into account the fact that less complicated layouts are more preferred due to space and weight limits in mechanical structures, all absorber layouts with no more than one damper, inerter and spring each are considered as candidate layouts. Because neither an inerter nor a spring can dissipate energy, a damper must be present in each candidate layout. Apart from a viscous damper only, there are in total four two-element and eight three-element absorber layouts that contain one damper, which then cover all layouts that need to be considered. These are respectively shown in Fig. 2 and Fig. 3. For each layout, one terminal is connected to the cable at mass a_f and the other is attached to a fixed support. The admittance functions of all candidate absorber layouts are summarized in Table 1.

For generality, the parameters of the absorber layouts are presented in non-dimensional form. Here, the non-dimensional inertance, damping coefficient and stiffness of the absorber elements are defined as $b' = b/M$, $c' = (c/M)/(\omega_o/\pi)$ and $k' = (k/M)/(\omega_o/\pi)^2$ respectively. The circular natural frequencies ω_e of the damped system and the location of the damper relative to the total length of the cable a_f are also presented in non-dimensional form as $\omega' = \omega_e/\omega_o$ and $a'_f = a_f/(n+1)$, respectively. Since the location of all candidate absorbers has been set to be at 5% length of the whole cable, thus $a'_f = 0.05$.

Two performance measures

Two different performance measures are used for optimization analysis in the present study. For shorter cables, the lowest frequency mode (i.e. the first mode) is often susceptible to vibrations, while vibrations of other modes can be neglected (Gimsing and Georgakis 2011). As the absorbers may affect the system's first natural frequency or introduce extra modes, it is proposed to consider

all modes in the frequency range from 0 to $1.5\omega_o$ to cover all modes in the vicinity of the first undamped mode of the cable. Therefore, the critical damping ratio ζ_c , which is defined as the lowest damping ratio of all modes in the frequency range from 0 to $1.5\omega_o$, is introduced as the key parameter to identify the effectiveness of the absorber layouts. The first performance measure is the optimum critical damping ratio denoted $\zeta_{c,opt}$ without considering higher frequency modes.

Since longer cables, or cables in extreme conditions, may suffer from vibrations in multiple modes, in some cases more low-frequency modes should be considered. Therefore, for the second performance measure, a constraint on the modes with higher frequencies is included. Hence, the second measure is $\zeta_{c,opt}$ with an extra constraint to ensure that the damping ratios of modes with natural frequencies in the range $[1.5\omega_o - 6.5\omega_o)$ are no less than those for a cable with a viscous damper optimized for the first mode. For simplicity, the damping ratios for the cable with a viscous damper are taken to be those from the universal curve (Pacheco et al. 1993).

For each performance measure, for a given non-dimensional inertance, the optimum critical damping ratio $\zeta_{c,opt}$ is found by using the Matlab optimization command ‘patternsearch’ followed by ‘fminsearch’ for fine-tuning of the parameters. The same approach has been used for optimizing absorbers for different applications (Smith and Wang 2004; Wang et al. 2009; Jiang et al. 2015b; Zhang et al. 2017; Li et al. 2017b). The maximum critical damping ratio $\zeta_{c,max}$ is defined as the maximum $\zeta_{c,opt}$, that can be achieved for any inertance.

Based on the lumped mass model with 99 DOFs, the results of the eigenvalue analysis for a viscous damper only (Layout I) are presented in Fig. 4 for a range of damping coefficients c' . Fig. 4a shows the relationship between critical damping ratio ζ_c and non-dimensional damping coefficient c' . This follows the universal curve (Pacheco et al. 1993), and similar results from other literatures (Krenk 2000; Main and Jones 2002). The optimum critical damping ratio $\zeta_{c,opt} = 0.0264$ is found by using the proposed optimization method, which matches with the maximum value on the curve, showing the validity of the proposed optimization approach. Fig. 4b shows the corresponding non-dimensional natural frequency ω' , which indicates that the viscous damper has marginal influence on the frequency of the first mode.

OPTIMUM PERFORMANCE OF CANDIDATE ABSORBERS

In this section, the optimum performance of all candidate absorbers is analyzed, with and without the constraint considering higher modes. Optimum critical damping ratios $\zeta_{c,opt}$ are identified, for all candidate layouts. For the layouts contain an inerter, inerters with non-dimensional inertance b' ranging from 0 to 2.5 are considered as this covers the maximum optimum critical damping ratio for all the layouts. Results for the beneficial absorber layouts are summarized compared. Since lower inertance is easier and typically less expensive to realize, more detailed discussions focus on b' from 0 to 0.5.

Optimization results for absorbers considering first mode only

As vibrations of the first mode are usually considered critical, this subsection aims to find the largest critical damping ratio ζ_c for the first mode without considering the effect on higher modes. All absorber layouts incorporating an inerter can provide a greater maximum optimum critical damping ratio than that for a viscous damper only, with suitable values of inertance. The optimization results for all candidate layouts are presented below.

Absorbers with two elements

For absorber layouts with two elements, layouts that can provide a larger maximum optimum critical damping ratio than a damper only are considered beneficial. The optimum critical damping ratios $\zeta_{c,opt}$ of both Layouts II-1 and II-2 (one damper in parallel or series with one spring), are found to be $\zeta_{c,opt} = 0.026$, which is the same as that for the viscous damper only. The corresponding non-dimensional damping coefficient and stiffness are respectively $c' = 6.430$, $k' = 0$ for Layout II-1 and $c' = 6.430$, $k' = \infty$ for Layout II-2 (i.e. both without the spring). In fact, for any tested c' in the range of 0 to 30, adding a spring always decreases the damping ratio for these two layouts. Therefore, these two layouts are not beneficial. Hence, only Layouts II-3 and II-4 (one damper in parallel or series with one inerter) are discussed below, together with the damper only (i.e. Layout I).

Fig. 5 presents a 3-D shaded surface plot of the critical damping ratio ζ_c for Layout II-3 with $0 \leq b' \leq 2.5$ and $0 \leq c' \leq 20$. The bold solid curve indicates the optimum critical damping

ratio for a given inertance. In Fig. 6a, the solid curve presents the optimum critical damping ratio as a function of the inertance, which corresponds to the bold solid curve in Fig. 5, while, the dashed curve shows the damping ratio for a simultaneously occurring non-critical mode also in the frequency range $0 < \omega' \leq 1.5$. The corresponding natural frequencies of both modes are shown in Fig. 6b. The lines for other layouts in Figs. 7-10 are consistent in style with those presented in Fig. 6.

As shown in Fig. 6a, with $b' = 0$, as expected, the optimized critical damping ratio is the same as that for a viscous damper only. For $b' > 0$, Layout II-3 provides a greater optimum critical damping ratio than that for a viscous damper only for any inertance b' investigated. It can be seen from the solid curve that among all the optimized results with varying b' , the maximum optimum critical damping ratio $\zeta_{c,max}$ is 0.155 for $b' = 1.760$, i.e. 5.9 times that for a viscous damper only. As b' increases from zero, the damping ratio of the original first mode (the mode with the lowest natural frequency, which is the initially the critical one) increases, but that of the original second mode decreases. At $b' = 1.760$, the damping ratios of the two modes are equal and above that value the damping ratio of the second mode is lower than that of the first mode, so the second mode becomes the critical one. It can be seen from Fig. 6b that the natural frequency of the second mode decreases as b' increases and at $b' = 1.760$ there is a switch of which mode is the critical one. It is notable that in all cases the natural frequency of the critical mode is similar to that of the original undamped first mode, showing that the frequency is not greatly influenced by the absorber. At $b' = 1.76$, the solutions for the critical and the non-critical modes cross over each other, which leads to the break point seen in Fig. 5 and Fig. 6a.

Fig. 7 presents the optimization results for Layout II-4. The results are of a similar form to those for Layout II-3. Layout II-4 is hence another beneficial layout compared with a viscous damper only if the non-dimensional inertance is sufficiently large. It can be seen from Fig. 7a that among all the optimized results with varying b' , Layout II-4 can provide $\zeta_{c,max} = 0.159$ for $b' = 2.250$, which is marginally better than the maximum for Layout II-3. However, Layout II-4 has the drawback that large optimum critical damping ratio $\zeta_{c,opt}$ cannot be achieved with relatively small b' . $\zeta_{c,opt}$ for

Layout II-4 is larger than that of a viscous damper if $b' > 1.15$. Similar to the case for Layout II-3, the break point at $b' = 2.250$ in Fig. 7a is due to a switch of which mode is the critical one and it can be seen in Fig. 7b that the natural frequency of the critical mode is always close to that of the original undamped first mode.

Absorbers with three elements

For all eight possible three element absorber layouts shown in Fig. 3, based on the optimization results, only Layouts III-3, III-4, III-5 and III-6 can provide greater optimum critical damping ratio $\zeta_{c,opt}$ than layouts with fewer elements (Layouts I, II-3 and II-4) with relatively small non-dimensional inertance b' . Among these four layouts, Layout III-6 is less preferable than the other three due to $\zeta_{c,opt}$ being lower for a wide range of b' . Therefore, only results for Layouts III-3, III-4 and III-5 are discussed and compared here.

It can be seen in Fig. 8 that among all the optimum results with varying b' , Layout III-3 can provide a maximum optimum critical damping ratio of $\zeta_{c,max} = 0.159$, for $b' = 2.250$, which is the same as Layout II-4, but Layout III-3 is more effective than Layout II-4 when $b' < 2.250$. For any optimum critical damping ratio with a given $b' \leq 2.250$, the two modes of the system with non-dimensional frequency $\omega' < 1.5$ provide the same damping ratio and very similar natural frequencies. This shows that the inerter and the spring provide a resonance to target the first mode. When $b' = 2.250$, the two modes bifurcate, since the corresponding non-dimensional stiffness reaches infinity. For $b' \geq 2.250$ the optimum results are the same as for Layout II-4, i.e. the spring in Layout III-3 has become a rigid connection.

The Layout III-4 is equivalent to a TMD when one terminal is grounded (Lazar et al. 2016). As shown in Fig. 9, among all the optimum results with varying b' , Layout III-4 can provide a maximum optimum critical damping ratio $\zeta_{c,max} = 0.159$, for non-dimensional inertance of $b' = 2.250$ (the same as for Layout II-4). However, compared with Layout II-4, Layout III-4 is more effective when b' is smaller. Similar to the results of Layout III-3, Layout III-4 also has the property that for any $\zeta_{c,opt}$ for given $b' \leq 2.250$, the two modes of the system with $\omega' \leq 1.5$ provide the same damping ratio and very similar natural frequencies. When $b' = 2.250$ the two modes bifurcate since the

non-dimensional stiffness k' for the optimum result reduces to zero. Since k' cannot physically be negative, for $b' > 2.250$, $\zeta_{c,opt}$ is the same as for Layout II-4.

It can be seen in Fig. 10 that among all the optimum results with varying non-dimensional inertance b' , Layout III-5 can provide $\zeta_{c,max} = 0.155$, for $b' = 1.760$, which is the same as for Layout II-3. Due to resonance provided by the inerter and spring, for $0.065 \leq b' \leq 1.760$, optimized results for Layout III-5 are better than those for Layout II-3. The two modes of the system with $\omega' < 1.5$ provide the same damping ratio and very similar frequencies. When $b' > 1.760$ or $b' < 0.065$, the optimized results for Layout III-5 are the same as those for Layout II-3, which lead to kinks in Fig. 10a. The optimum value of k' is then infinity, so the spring acts as a rigid link.

Optimization results for absorbers with the higher mode constraint

The optimization measures considering six modes is similar to that previously described, except that the additional constraint is implemented to consider the performance of higher modes. Optimization results show that for two-element layouts, Layouts II-3 and II-4 can provide better results than a viscous damper only, and for three element Layouts III-4 and III-6 perform better than the other three element layouts.

As shown in Fig. 11a, for Layout II-3 with non-dimensional inertance $b' = 0$, as expected, the optimized critical damping ratio is the same as that for a viscous damper only, i.e. $\zeta_{c,opt} = 0.026$. For $b' > 0.170$ the constraint affects the results, so $\zeta_{c,opt}$ is lower with the constraint than without it. For $b' > 0$, Layout II-3 provides a slightly greater optimum critical damping ratio than a damper only. It can be seen from the solid curve that among all the optimized results with varying b' , $\zeta_{c,max}$ is 0.028 for $b' = 0.160$. When optimized with $b' < 0.170$ without the constraint, the damping ratio of the higher modes are all above the constraint. Therefore, results both with and without the constraint are the same. In Fig. 11b, the crosses show the damping ratio for the higher modes for the optimized system with $b' = 0.195$. The optimum critical damping ratio $\zeta_{c,opt}$ is restricted by the damping ratio of the sixth mode, which is on the boundary provided by the solution of the viscous damper. However, for $b' > 0.195$, the sixth mode cannot meet the boundary condition that no worse than that for a viscous damper optimized for the first mode. Therefore, the solid curve in

Fig. 11a terminates. Similar situations can occur for the other layouts.

Fig. 11c shows the optimization results for Layout II-4. The maximum optimum critical damping ratio $\zeta_{c,max}$ with the constraint is 0.062 for $b' = 2.172$, which is much greater than for a damper only, but large inertance is required. The solid curve starts at $b' = 0.390$ since for small b' the damping ratio of the second mode cannot satisfy the constraint. For $b' > 1.500$, the optimum solution is limited by the sixth mode, giving reduced result compared with the case without the constraint.

Based on the optimization results, it is found that with suitable amount of inertance, all candidate layouts with three elements can provide greater $\zeta_{c,opt}$ than layouts with fewer elements (i.e. Layouts I, II-3 and II-4). Since Layouts III-4 and III-6 are the most beneficial ones, therefore, their results are discussed in detail below.

Fig. 12a shows the optimization results for Layout III-4. The maximum optimum critical damping ratio $\zeta_{c,max}$ is 0.141 for $b' = 1.47$. The solid curve allowing the additional constraint starts at $b' = 0.390$ since below that the damping ratio of the second mode cannot satisfy the constraint. For $b' < 0.90$, the optimum solution is limited by the second mode and for $b' > 1.40$ it is limited by the sixth mode. For $0.9 \leq b' \leq 1.4$, the results are not limited by the additional constraint, so the optimum solution is the same as when only considering the critical damping ratio.

Fig. 12b shows the optimization results for Layout III-6. The maximum optimum critical damping ratio $\zeta_{c,max}$ is 0.033 for $b' = 0.215$. When $b' < 0.070$, the corresponding k' becomes a rigid connection, and it can be simplified to Layout II-3. For $b' > 0.340$, since the corresponding stiffness $k' = 0$, Layout III-6 reduce to a damper only, so there is no further change in $\zeta_{c,opt}$.

Summary for all beneficial layouts

Although inerters can realize large inertance by using gearing, with relatively small actual mass (Smith 2002), in practice it is difficult and currently uneconomical to realize an inerter with extremely large inertance. Therefore, only two element layouts that can provide better optimum critical damping ratio than a damper only, and some most beneficial three element layouts with relatively small non-dimensional inertance within the range, $0 \leq b' \leq 0.5$, are compared and

illustrated in Figures.

For all absorber layouts without the higher modes constraint, Layouts II-3, II-4, III-3, III-4 and III-5 are considered beneficial. The performance improvements for these five layouts, including their beneficial inertance region, maximum improvement compared with a damper only (in percentage terms) and the maximum benefit for $0 \leq b' \leq 0.5$ are summarized in Table 2.

For $b' \leq 0.5$ the optimum critical damping ratios $\zeta_{c,opt}$ of Layouts II-3 and II-4, and their corresponding non-dimensional damping coefficients c' are compared in Fig. 13, along with the results for a damper only. Layout II-3 provides higher $\zeta_{c,opt}$ than Layout II-4 and a damper only in this range. Also, a lower damping coefficient is required than that of Layout I. Layout II-4 is only more beneficial than Layout II-3 for $b' > 1.950$ and it can provide a slightly better maximum optimum critical damping ratio $\zeta_{c,max} = 0.159$ compared with $\zeta_{c,max} = 0.155$ for Layout II-3. However, for $0 \leq b' \leq 0.5$, only Layout II-3 is beneficial. Up to 34% increase in the critical damping ratio can be realized compared with a viscous damper only by Layout II-3, as shown in Table 2.

Without the higher mode constraint, the optimization results of the beneficial three-element absorber layouts, i.e. Layouts III-3, III-4 and III-5, are shown in Fig. 14 for $b' < 0.5$. Layout III-4 provides the largest optimum damping ratio $\zeta_{c,opt}$ over a wide range of non-dimensional inertance values b' , though the difference with the other two layouts are often small. For $b' \leq 0.065$, Layout III-5 is most beneficial where it reduces to Layout II-3. For $b' > 0.065$, Layout III-5 provides different solutions with greater $\zeta_{c,opt}$, which leads to the jump in c' in Fig. 14. For $0.065 < b' \leq 0.5$, there is little difference in performance between the three element layouts, while much lower non-dimensional damping coefficients c' are required for Layouts III-4 and III-5 compared with III-3. Fig. 14c shows that the corresponding non-dimensional stiffness k' are about π^2 times b' for all three layouts, indicating that the inerter and spring provide resonance to target the first mode.

With the higher mode constraint, only Layouts II-3, II-4, III-4 and III-6 are considered beneficial. The performance improvements of these four layouts are summarized in Table 3. The optimization

results show that Layout III-6 in the range $0 \leq b' \leq 0.510$ and III-4 in the range $0.510 \leq b' \leq 2.5$ provides more beneficial optimized critical damping ratios than the other layouts. Layout III-4 provides the overall optimum critical damping ratio, while Layout III-6 is still worth considering in practice, since it provides reasonable benefits with relatively small inertance. As is shown in Fig. 15, only Layouts II-3 and III-6 can provide results better than a viscous damper for $b' \leq 0.5$. Compared with the results without the constraint, c' and k' are of the same order of magnitude, but the higher mode constraint has greatly reduced $\zeta_{c,opt}$ for all the beneficial absorber layouts.

EFFECTS OF SERIES COMPLIANCE

In practice, the connections at either end of the absorber, with the support and with the cable, may not be fully rigid. Apart from compliance of the connections themselves and of any axial linkage element, for common bridge cables made up of multiple parallel strands in an outer sheath, there may be relative movement between the sheath, to which the absorber is usually attached, and the structural strands inside. The lack of rigidity may be expected to reduce the performance of the absorber. In order to quantify this effect, a compliant element is introduced in series with the absorber. For simplicity, it is modeled as an ideal spring of non-dimensional stiffness k'_{sc} . The upper limit of possible stiffness values is considered infinite. The lower realistic limit is estimated using simplified assumptions. For vibrations of the main length of the cable (from the absorber to the other end) in a half sine wave mode shape, neglecting motion of the point where the absorber is attached and the short length of cable between that point and the near end, the force on the absorber is given approximately by $T\theta_{af}$ (Fig. 1). The maximum value of θ_{af} approximately equals $\pi x_{max}/L$, where x_{max} is the maximum displacement at the anti-node of the mode. If this force causes a deformation between the end of the absorber and the cable γ , the equivalent linear stiffness of the series spring, k_{sc} , is $T\pi x_{max}/(L\gamma)$. Hence the non-dimensional stiffness k'_{sc} is simply $\pi x_{max}/\gamma$. Typically, it is aimed for x_{max} to be limited to the diameter of the cable, which is typically about 200mm, whilst the deformation γ is estimated to be of the order of 10mm. Hence the minimum value of k'_{sc} in practice is estimated to be around 60. Therefore, to more than cover the range of expected values, in this study k'_{sc} is taken to be in the range of 10 to infinity.

The effects of series compliance are analyzed for both performance measures, with and without the higher mode constraint. The higher mode constraint used here is the performance of a viscous damper with the same series compliance, rather than the universal curve used in previous sections. The beneficial layouts with two elements, i.e., Layouts II-3 and II-4, are not discussed here, as the optimization results show that both layouts cannot achieve the same level of critical damping ratio when series compliance is included. The effect of k'_{sc} on the beneficial layouts with three elements, i.e. Layouts III-3_{sc}, III-4_{sc}, III-5_{sc} and III-6_{sc}, are investigated. The four layouts, including the series compliance, are shown in Fig. 16.

Using the previously optimized parameter values, when the series compliance is added the critical damping ratios decrease significantly for all four layouts. Given the detrimental effect, the parameters of the absorbers should be re-optimized.

Layouts III-3_{sc} and III-5_{sc} have two springs in series. Therefore, if $k'_{sc} \geq k'_o$, where k'_o is the original optimized non-dimensional stiffness without series compliance, they can be adjusted to have identical properties to the original optimized layouts. The re-tuned k' can simply be calculated as $k' = 1/[(1/k'_o) - (1/k'_{sc})]$. Since k' increases with b' (Fig. 14c), this is possible for b' up to a certain value, $b' < b'_m$, at which $k'_{sc} = k'_o$, and the maximum value of $\zeta_{c,opt}$ can be achieved. For $b' > b'_m$ the performance of Layouts III-3_{sc} and III-5_{sc} rapidly decreases, but it is still larger than that of without retuning k' .

For Layout III-4_{sc} the two springs are not simply in series, so re-optimization of the absorber layout is needed. Fig. 17a shows that, without re-optimization and without considering the higher mode constraint, for k'_{sc} equal to 10, 100 and 1000, the maximum optimum critical damping ratio $\zeta_{c,max}$ respectively are 83.0%, 47.2% and 2.7% of the original $\zeta_{c,max}$ only. Similar results have also been found for Layouts III-3_{sc}, III-5_{sc} and III-6_{sc}. The re-optimized results for Layout III-4_{sc} are shown in Fig. 17b for the k'_{sc} equal to 10, 100 and 1000, as well as infinity. In each case, for b' up to a certain value b'_m , indicated by crosses, the optimum critical damping ratio of the re-optimized layout is at least as great as for the original layout. To achieve the optimum behavior, both the non-dimensional damping coefficient c' and non-dimensional stiffness k' need to be adjusted. For

$b' > b'_m$, the re-optimized $\zeta_{c,opt}$ for Layout III-4_{sc} cannot reach the original value, but it is still better than that without re-optimization.

Fig. 18 shows the relation of the maximum critical inertance b'_m and the corresponding optimum critical damping ratio $\zeta_{c,opt}$ to the series compliance k'_{sc} for Layouts III-3_{sc}, III-4_{sc} and III-5_{sc}. For all three layouts, when relatively stiff series compliance is considered, i.e. $k'_{sc} \geq 100$, only a marginal effect on $\zeta_{c,opt}$. When very soft series compliance is considered, taking the worst case of $k'_{sc} = 10$ as example, the re-optimized $\zeta_{c,opt}$ still reaches 60% of the original $\zeta_{c,max}$. Also, when $k'_{sc} = 10$, the maximum critical non-dimensional inertance $b'_m \approx 0.6$ for all three layouts, indicating that within the range of inertance of most interest ($b' \leq 0.5$), the same or even marginally better $\zeta_{c,opt}$ can be achieved compared with the case without the series compliances.

Considering the higher mode constraint, Layout III-6_{sc} cannot reach the original optimum even if the absorber is returned. However, it is still much more beneficial than the case where the parameters are not retuned. For Layout III-4, the re-optimized results are presented in Fig. 19, showing that softer k'_{sc} can be beneficial if the system is returned. For a range of b' , which depends on k'_{sc} , the re-optimized system can still provide a critical damping ratio as good as, and in some cases significantly greater than the critical damping ratio provided by the original layout.

CONCLUSIONS

In this paper, a systematic approach to identify beneficial low-complexity inerter-based absorber layouts for cable vibration suppression is presented. A Finite Element (FE) model of the cable is firstly presented with various absorber layouts represented by admittance functions. Then, considering the first mode only and the first six modes, two performance measures are proposed. Based on the model, absorbers with different layouts are optimized. The performance of all possible absorber layouts with no more than one inerter, damper and spring is analyzed with non-dimensional inertance b' within the range of 0 to 2.5, with further focus on the more practical range of 0 to 0.5. The results show that all layouts incorporating with inerters can provide more beneficial optimum critical damping ratios than for a viscous damper only. Compared with two-element layouts for small inertance, three-element layouts can provide greater damping. Considering only the critical

damping ratio, three layouts with three elements are found to be most beneficial, offering much greater damping ratios than other layouts when the inerter is small. Including the higher mode constraint, two three-element layouts are found to be most beneficial, even though their performance is restricted by the constraint. Finally, the effects of series compliance are analyzed for the most beneficial layouts, showing that without re-optimization the series compliance is detrimental, as expected. However, up to a certain inertance, which depends on the series compliance, the absorbers can provide virtually the same, or in some cases even better performance as without the series compliance if the element values are properly retuned.

ACKNOWLEDGEMENTS

This work was supported by the EPSRC and the China Scholarship Council: Jason Zheng Jiang is supported by an EPSRC Grant EP/P013456/1; Jiannan Luo is supported by the Chinese Scholarship Council for his PhD study.

REFERENCES

- Bakis, K., Massaro, M., Williams, M., and Graham, J. (2017). "Passive control of bridge wind-induced instabilities by tuned mass dampers and movable flaps." *Journal of Engineering Mechanics*, 143(9), 04017078.
- Brune, O. (1931). "Synthesis of a finite two-terminal network whose driving-point impedance is a prescribed function of frequency." *Studies in Applied Mathematics*, 10(1-4), 191–236.
- Caetano, E. (2007). *Cable vibrations in cable-stayed bridges*. Int. Association for Bridge and Structural Engineering, Zurich, Switzerland.
- Cai, C., Wu, W., and Shi, X. (2006). "Cable vibration reduction with a hung-on tmd system. part I: Theoretical study.." *Journal of Vibration and Control*, 12(7), 801–814.
- Cu, V. and Han, B. (2015). "A stay cable with viscous damper and tuned mass damper." *Australian Journal of Structural Engineering*, 16(4), 316–323.
- Den Hartog, J. (1933). "Transmission line vibration due to sleet." *Transactions of the American Institute of Electrical Engineers*, 51(4), 1074–1076.

- Gimsing, N. and Georgakis, C. (2011). *Cable supported bridges: concept and design (3rd edition)*. Wiley & Sons, London, UK.
- Hikami, Y. and Shiraishi, N. (1988). “Rain-wind induced vibrations of cables in cable-stayed bridges.” *Journal of Wind Engineering and Industrial Aerodynamics*, 29, 409–418.
- Ikago, K., Saito, K., and Inoue, N. (2012). “Seismic control of single-degree-of-freedom structure using tuned viscous mass damper.” *Earthquake Engineering and Structural Dynamics*, 41, 453–474.
- Jiang, J., Liu, X., and Harrison, A. (2015a). “Passive suspension incorporating inerters for road damage improvement of heavy vehicles.” *Symposium on Dynamics of Vehicles on Road and Tracks*, Graz, Austria.
- Jiang, J., Matamoros-Sanchez, A., Zolotas, A., Goodall, R., and Smith, M. (2015b). “Passive suspensions for ride quality improvement of two-axle railway vehicles.” *Proceedings of Mechanical Engineering Part F: Journal of Rail and Rapid Transit*, 229, 315–329.
- Krenk, S. (2000). “Vibrations of a taut cable with an external damper.” *Journal of Applied Mechanics*, 67(4), 772–776.
- Lazar, I., Neild, S., and Wagg, D. (2014). “Using an inerter-based device for structural vibration suppression.” *Earthquake Engineering & Structural Dynamics*, 43(8), 1129–1147.
- Lazar, I., Neild, S., and Wagg, D. (2016). “Vibration suppression of cables using tuned inerter dampers.” *Engineering Structures*, 122, 62–71.
- Li, Y., Howcroft, C., Jiang, J., and Neild, S. (2017a). “Using continuation analysis to identify shimmy-suppression devices for an aircraft main landing gear.” *Journal of Sound and Vibration*, 408, 234–251.
- Li, Y., Jiang, J., and Neild, S. (2017b). “Inerter-based configurations for main landing gear shimmy suppression.” *Journal of Aircraft*, 54, 684–693.
- Lilien, J. and Da Costa, A. (1994). “Vibration amplitudes caused by parametric excitation of cable stayed structures.” *Journal of Sound and Vibration*, 174(1), 69–90.
- Liu, Y., Chen, M., and Tian, Y. (2015). “Nonlinearities in landing gear model incorporating inerter.”

- 525 *IEEE International Conference on Information and Automation*, 696–701.
- 526 Macdonald, J. (2016). “Multi-modal vibration amplitudes of taut inclined cables due to direct
527 and/or parametric excitation.” *Journal of Sound and Vibration*, 363, 473–494.
- 528 Macdonald, J. and Larose, G. (2006). “A unified approach to aerodynamic damping and drag/lift
529 instabilities, and its application to dry inclined cable galloping.” *Journal of Fluids and Structures*,
530 22(2), 229–252.
- 531 Main, J. and Jones, N. (2002). “Free vibrations of taut cable with attached damper. I: Linear viscous
532 damper.” *Journal of Engineering Mechanics*, 128(10), 1062–1071.
- 533 Makris, N. and Kampas, G. (2016). “Seismic protection of structures with supplemental rotational
534 inertia.” *Journal of Engineering Mechanics*, 142(11), 04016089.
- 535 Matsumoto, M., Shiraishi, N., Kitazawa, M., Knisely, C., Shirato, H., Y., K., and Tsujii, M. (1990).
536 “Aerodynamic behaviour of inclined circular cylinders-cable aerodynamics.” *Journal of Wind*
537 *Engineering and Industrial Aerodynamics*, 33(1-2), 63–72.
- 538 Pacheco, B., Fujino, Y., and Sulekh, A. (1993). “Estimation curve for modal damping in stay cables
539 with viscous damper.” *Journal of Structural Engineering*, 119(6), 1961–1979.
- 540 Smith, M. (2002). “Synthesis of mechanical networks: The inerter.” *IEEE Transactions on Auto-*
541 *matic Control*, 47(10), 1648–1662.
- 542 Smith, M. and Wang, F. (2004). “Performance benefits in passive vehicle suspensions employing
543 inerters..” *Vehicle System Dynamics*, 42(4), 235–257.
- 544 Tokoroa, S., Komatsub, H., Nakasub, M., Mizuguchic, K., and Kasugad, A. (2000). “A study on
545 wake-galloping employing full aeroelastic twin cable model.” *Journal of Wind Engineering and*
546 *Industrial Aerodynamics*, 88, 247–261.
- 547 Wang, F., Hsieh, M., and Chen, H. (2012). “Stability and performance analysis of a full-train system
548 with inerters.” *Vehicle System Dynamics*, 50(4), 545–571.
- 549 Wang, F., Liao, M., Liao, B., Su, W., and Chan, H. (2009). “The performance improvements of train
550 suspension systems with mechanical networks employing inerters.” *Vehicle System Dynamics*,
551 47(7), 805–830.

- 552 Yang, J. (2016). “Force transmissibility and vibration power flow behaviour of inerter-based vibra-
553 tion isolators.” *13th International Conference on Motion and Vibration Control (MOVIC 2016)*
554 *joint with the 12th International Conference on Recent Advances in Structural Dynamics (RASD)*,
555 Southampton, UK.
- 556 Zhang, Y., Jiang, J., and Neild, S. (2017). “Optimal configurations for a linear vibration suppression
557 device in a multi-storey building.” *Structural Control and Health Monitoring*, 24.

558	List of Tables	
559	1	Admittance function $Y(s)$ for all candidate absorbers 24
560	2	Relative improvement of beneficial layouts without higher mode constraint 25
561	3	Relative improvement of beneficial layouts considering constraint of higher modes . 26

TABLE 1. Admittance function $Y(s)$ for all candidate absorbers

Layout	Admittance function	Layout	Admittance function
I	c	III-3	$1/[(1/bs) + (1/c) + (s/k)]$
II-1	$c + k/s$	III-4	$1/[1/(c + k/s) + (1/bs)]$
II-2	$1/[(1/c) + (s/k)]$	III-5	$1/[1/(c + bs) + (s/k)]$
II-3	$bs + c$	III-6	$1/[(1/bs) + (s/k)] + c$
II-4	$1/[(1/c) + (1/bs)]$	III-7	$1/[(s/k) + (1/c)] + bs$
III-1	$1/[(1/c) + (1/bs)] + (k/s)$	III-8	$bs + c + k/s$
III-2	$1/[1/(bs + k/s) + c]$		

TABLE 2. Relative improvement of beneficial layouts without higher mode constraint

Beneficial layout	Range of beneficial b'	Maximum improvement $b' \in (0, 2.5]$	Corresponding b'	Maximum improvement $b' \in (0, 0.5]$	Corresponding b'
II-3	(0, 2.5]	487%	1.760	34%	0.5
II-4	(1.150, 2.5]	502%	2.250	N/A	N/A
III-3	(0.080, 2.25]	502%	2.250	196%	0.5
III-4	(0, 20.25]	502%	2.250	203%	0.5
III-5	(0, 20.5]	487%	1.760	202%	0.5

TABLE 3. Relative improvement of beneficial layouts considering constraint of higher modes

Beneficial layout	Range of beneficial b'	Maximum improvement $b' \in (0, 2.5]$	Corresponding b'	Maximum improvement $b' \in (0, 0.5]$	Corresponding b'
II-3	(0, 2.5]	8.96%	0.160	8.96%	0.160
II-4	(1.150, 2.5]	150%	2.25	N/A	N/A
III-4	(0.080, 2.25]	451%	2.25	N/A	N/A
III-6	(0, 2.25]	27.6%	0.215	27.6%	0.215

List of Figures

1	Finite element model of a taut cable with an absorber	29
2	Candidate absorber layouts with one or two elements	30
3	Candidate absorber layouts with three elements	31
4	Results for Layout I (viscous damper only). (a) Critical damping ratio and (b) corresponding non-dimensional natural frequency, versus non-dimensional damping coefficient	32
5	3-D plot of damping ratio versus non-dimensional inertance and damping coefficient for Layout II-3	33
6	Optimization results for Layout II-3. (a) Damping ratio and (b) corresponding non-dimensional frequency, versus non-dimensional inertance	34
7	Optimization results for Layout II-4. (a) Damping ratio and (b) corresponding non-dimensional frequency, versus non-dimensional inertance	35
8	Optimization results for Layout III-3. (a) Damping ratio and (b) corresponding non-dimensional frequency, versus non-dimensional inertance	36
9	Optimization results for Layout III-4. (a) Damping ratio and (b) corresponding non-dimensional frequency, versus non-dimensional inertance	37
10	Optimization results for Layout III-5. (a) Damping ratio and (b) corresponding non-dimensional frequency, versus non-dimensional inertance	38
11	Performance of two element layouts with and without the constraint. (a) Damping ratio for Layout II-3 versus non-dimensional inertance. (b) Damping ratios for Layout II-3 for higher modes optimized when $b' = 0.195$. (c) Damping ratio for Layout II-4 versus non-dimensional inertance	39
12	Optimized damping ratio versus non-dimensional inertance with and without the constraint. (a) Layout III-4 and (b) Layout III-6, optimum critical damping ratio versus non-dimensional inertance	40

588	13	Optimization results for beneficial layouts with one or two elements without the	
589		higher mode constraint. (a) Damping ratio and (b) corresponding non-dimensional	
590		damping coefficient, versus non-dimensional inertance	41
591	14	Optimization results for beneficial layouts with three elements without the higher	
592		mode constraint. (a) Damping ratio, (b) corresponding non-dimensional damp-	
593		ing coefficient and (c) corresponding non-dimensional frequency, versus non-	
594		dimensional inertance	42
595	15	Optimization results for beneficial layouts with the higher mode constraint. (a)	
596		Damping ratio, (b) corresponding non-dimensional damping coefficient and (c)	
597		corresponding non-dimensional frequency, versus non-dimensional inertance . . .	43
598	16	Beneficial three-element layouts with added series compliance	44
599	17	Critical damping ratios with different series compliance (k'_{sc}) for Layout III-4 _{sc} (a)	
600		with original optimized parameters (b) with re-optimized parameters	45
601	18	Optimization results for Layouts III-3 _{sc} , III-4 _{sc} and III-5 _{sc} . (a) Maximum critical	
602		inertance b'_m and (b) corresponding optimum critical damping ratio $\zeta_{c,opt}$, versus	
603		non-dimensional series compliance	46
604	19	Optimum critical damping ratio for Layout III-4 _{sc} , versus non-dimensional iner-	
605		tance for re-optimized results with the constraint of higher mode and different series	
606		compliance	47

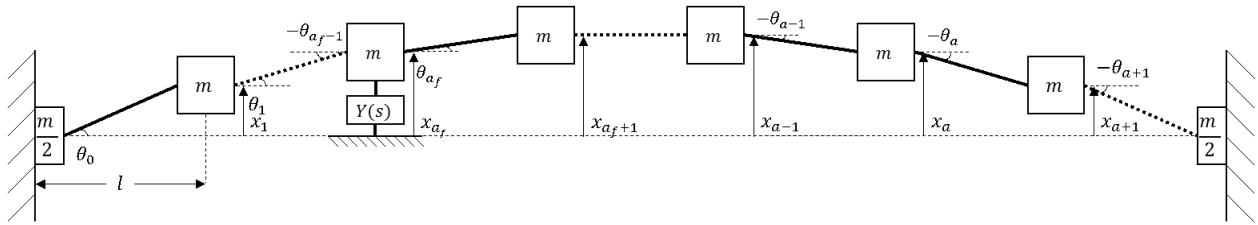


Fig. 1. Finite element model of a taut cable with an absorber

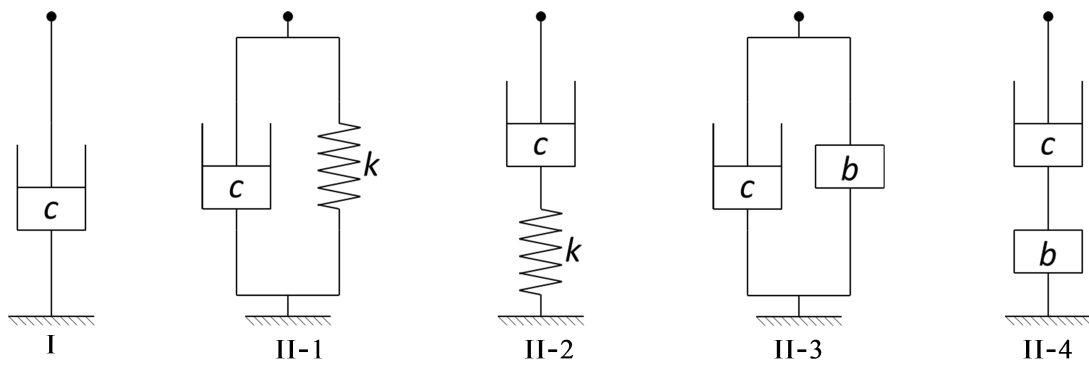


Fig. 2. Candidate absorber layouts with one or two elements

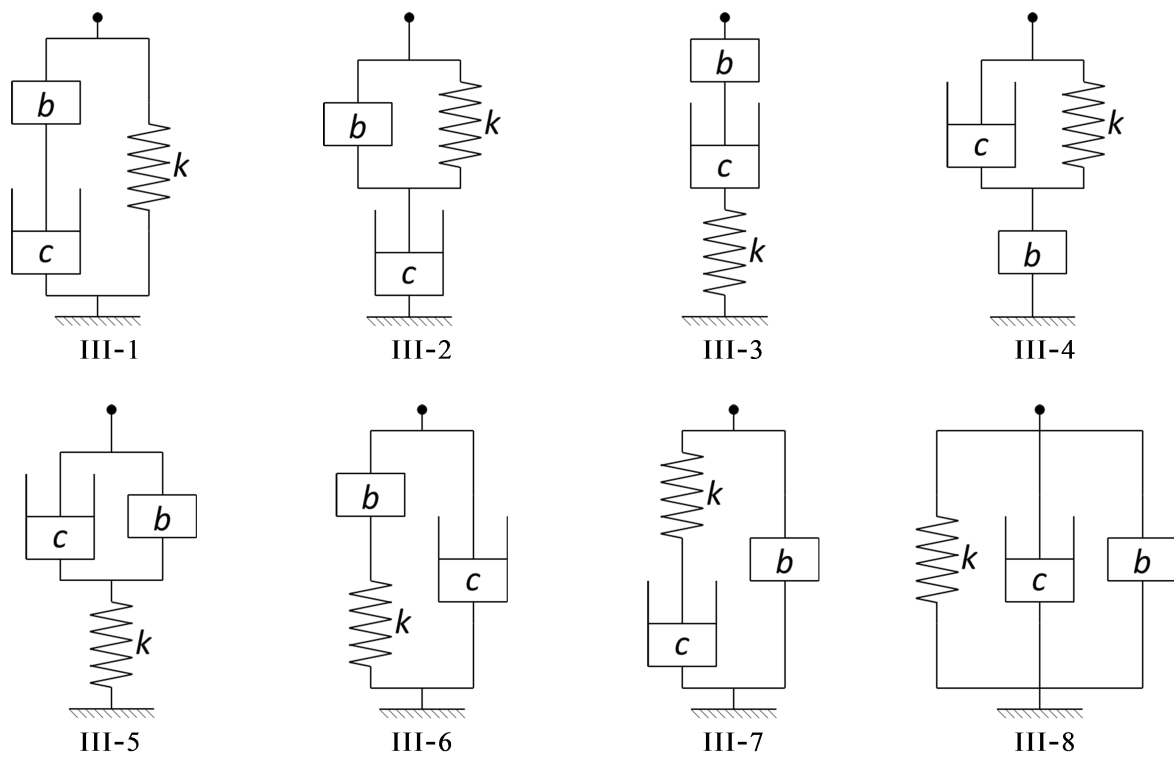


Fig. 3. Candidate absorber layouts with three elements

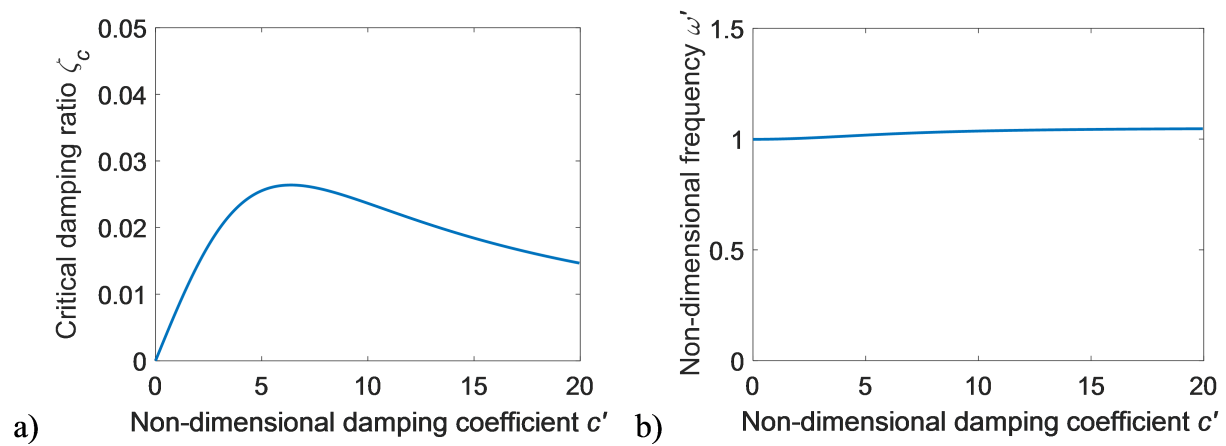


Fig. 4. Results for Layout I (viscous damper only). (a) Critical damping ratio and (b) corresponding non-dimensional natural frequency, versus non-dimensional damping coefficient

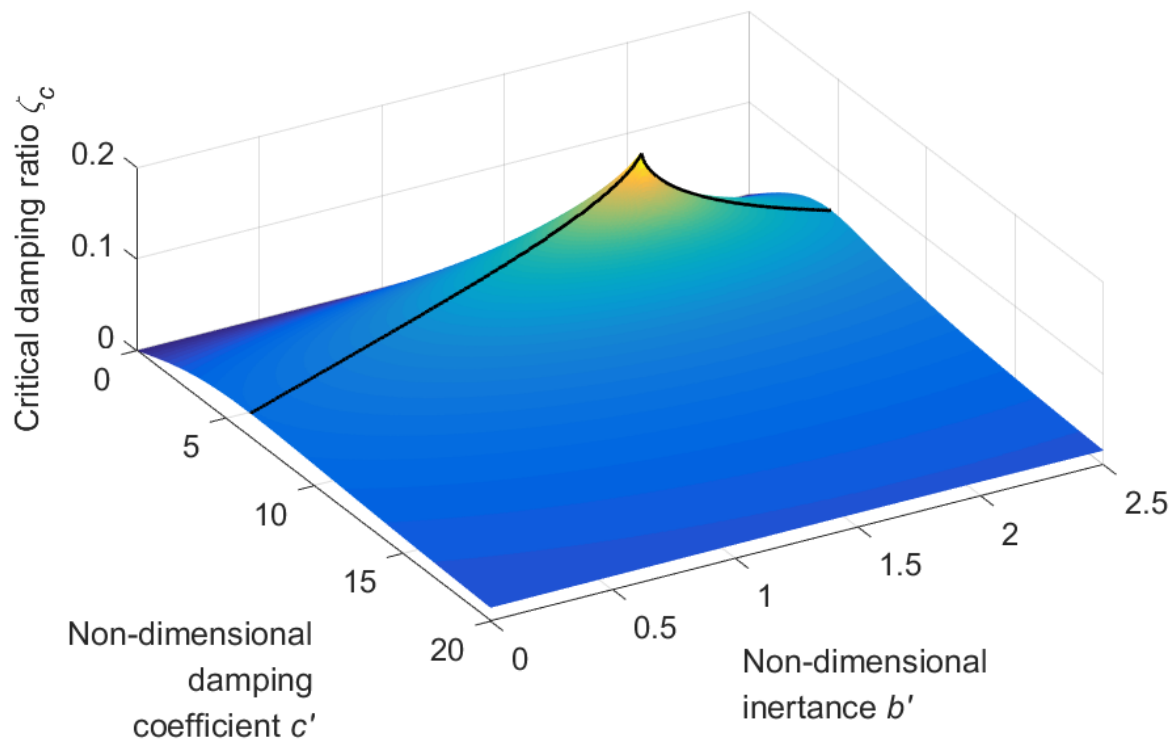


Fig. 5. 3-D plot of damping ratio versus non-dimensional inertance and damping coefficient for Layout II-3

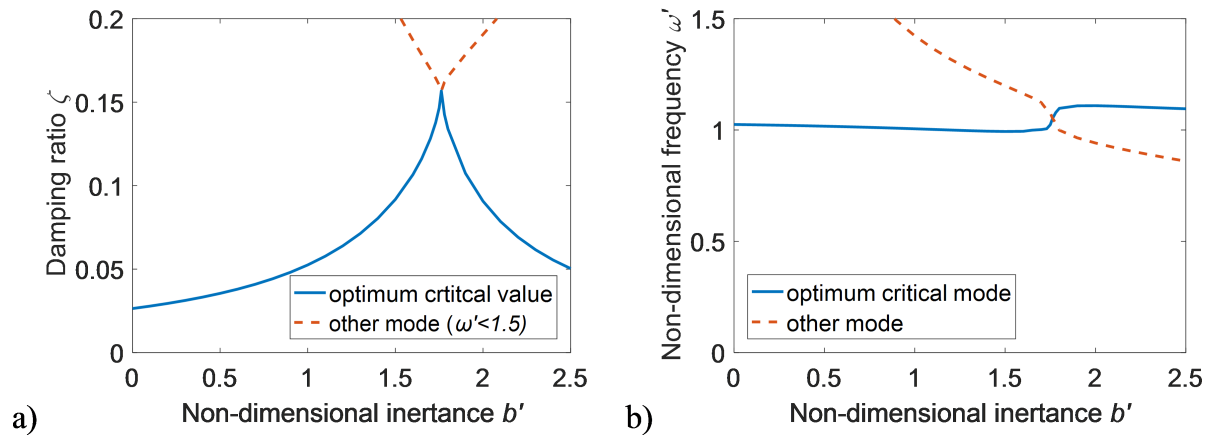


Fig. 6. Optimization results for Layout II-3. (a) Damping ratio and (b) corresponding non-dimensional frequency, versus non-dimensional inertance

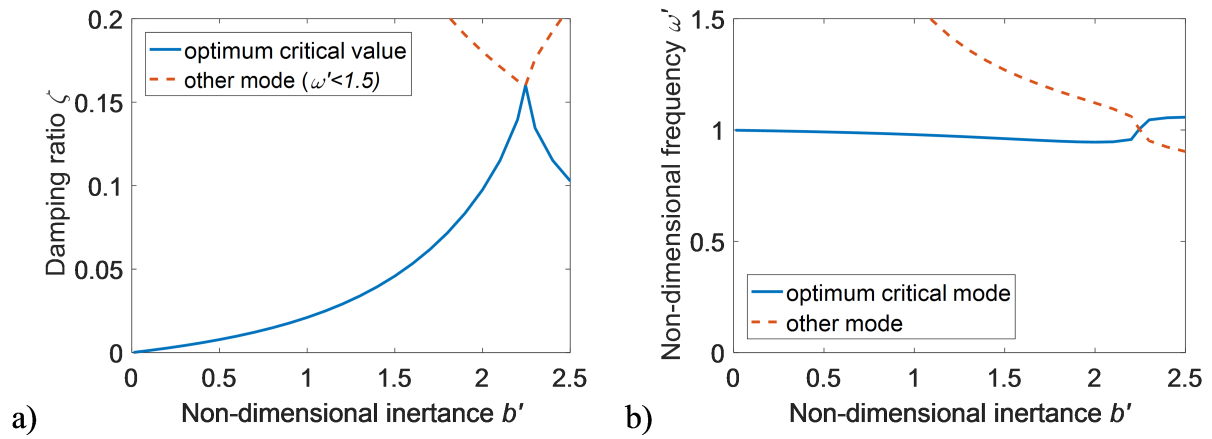


Fig. 7. Optimization results for Layout II-4. (a) Damping ratio and (b) corresponding non-dimensional frequency, versus non-dimensional inertance

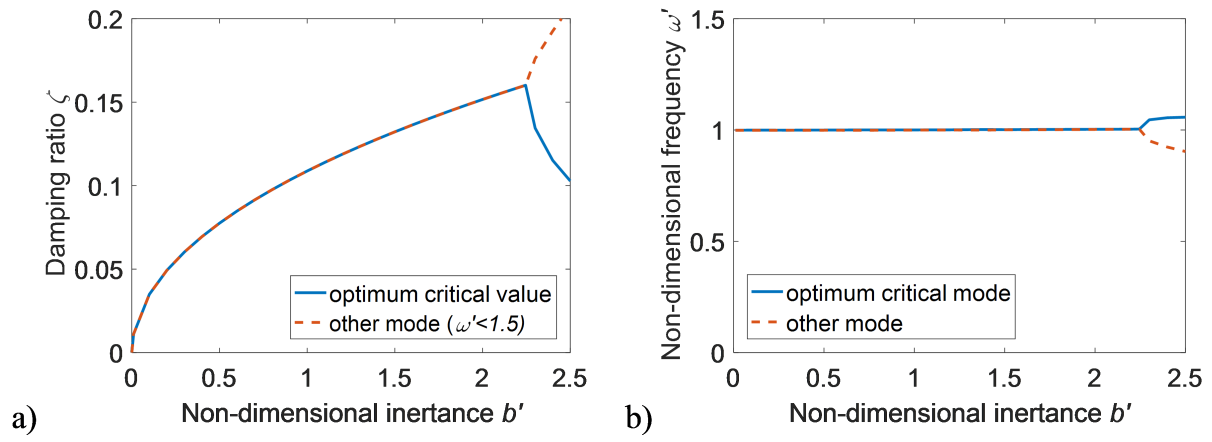


Fig. 8. Optimization results for Layout III-3. (a) Damping ratio and (b) corresponding non-dimensional frequency, versus non-dimensional inertance

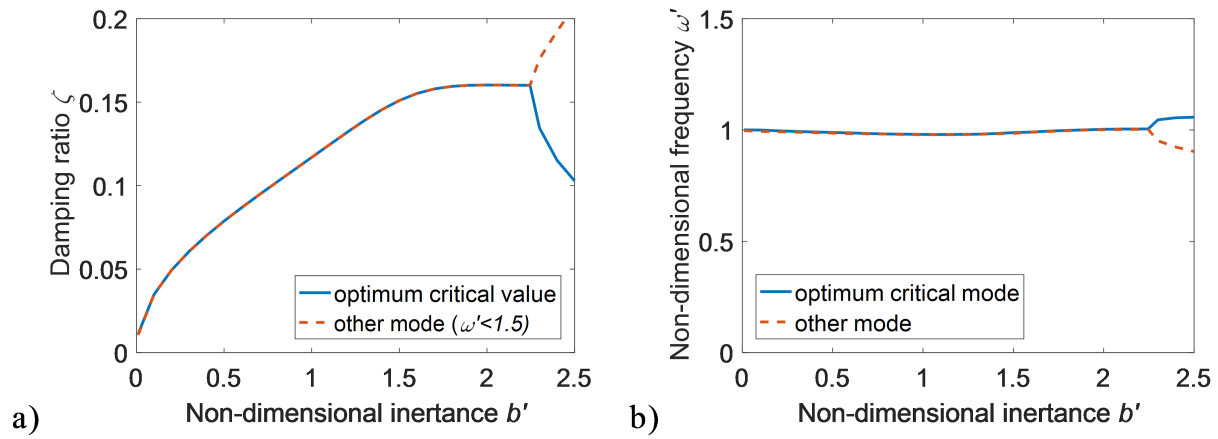


Fig. 9. Optimization results for Layout III-4. (a) Damping ratio and (b) corresponding non-dimensional frequency, versus non-dimensional inertance

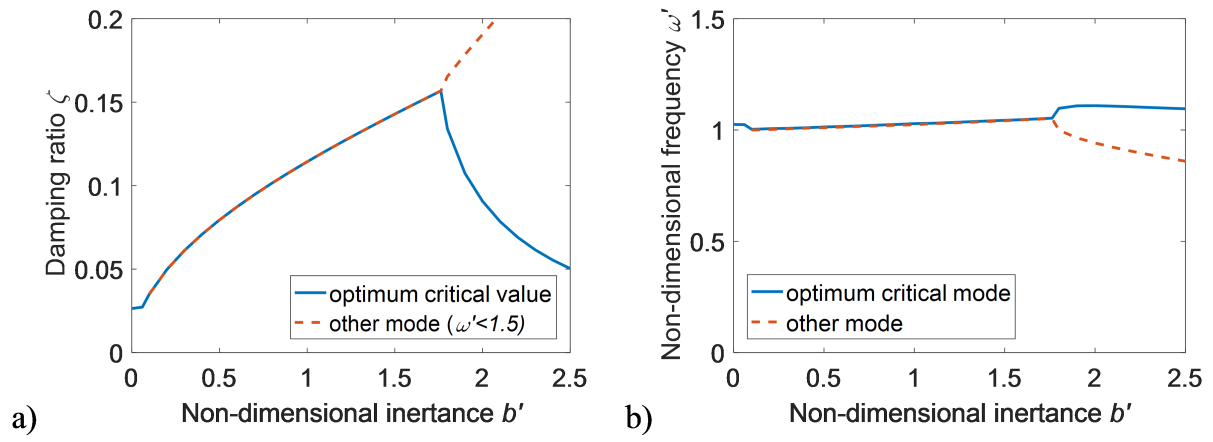


Fig. 10. Optimization results for Layout III-5. (a) Damping ratio and (b) corresponding non-dimensional frequency, versus non-dimensional inertance

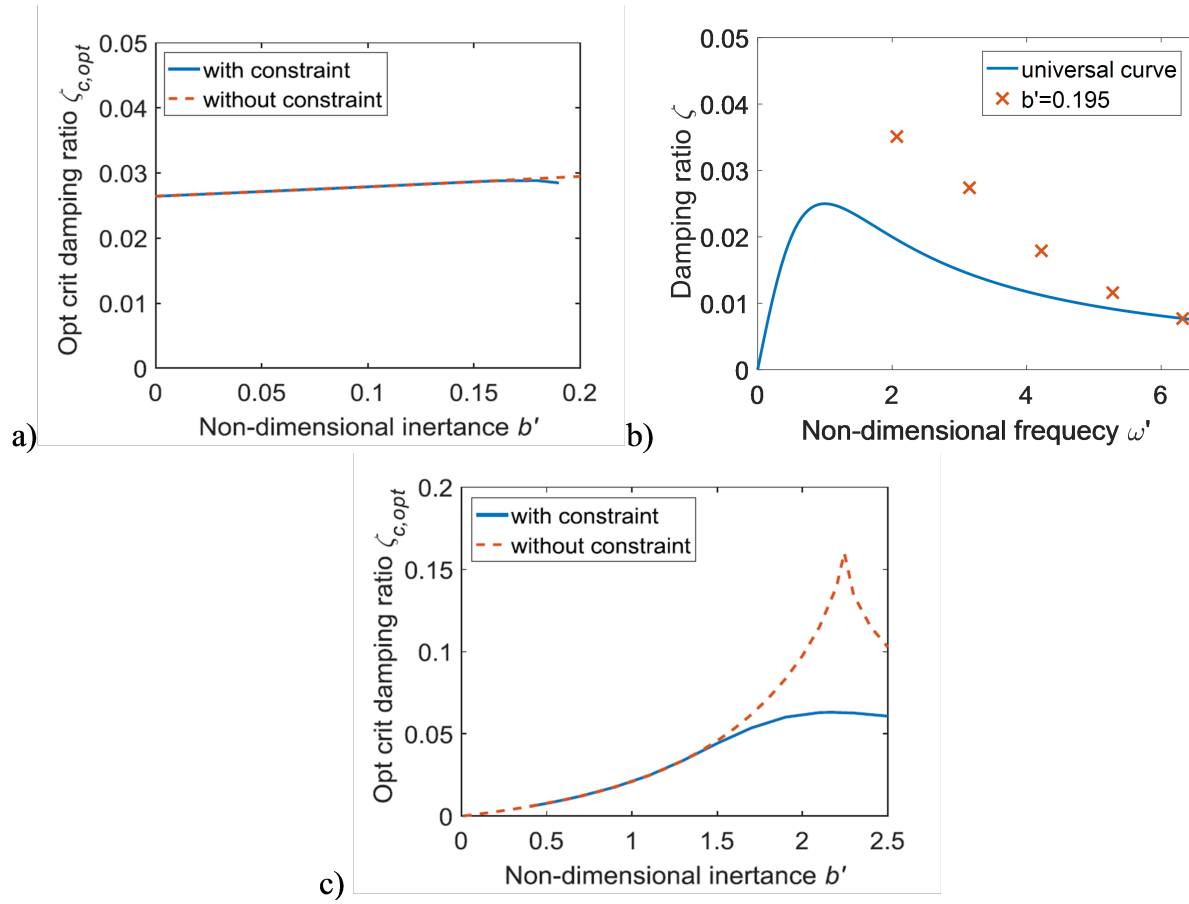


Fig. 11. Performance of two element layouts with and without the constraint. (a) Damping ratio for Layout II-3 versus non-dimensional inertia. (b) Damping ratios for Layout II-3 for higher modes optimized when $b' = 0.195$. (c) Damping ratio for Layout II-4 versus non-dimensional inertia

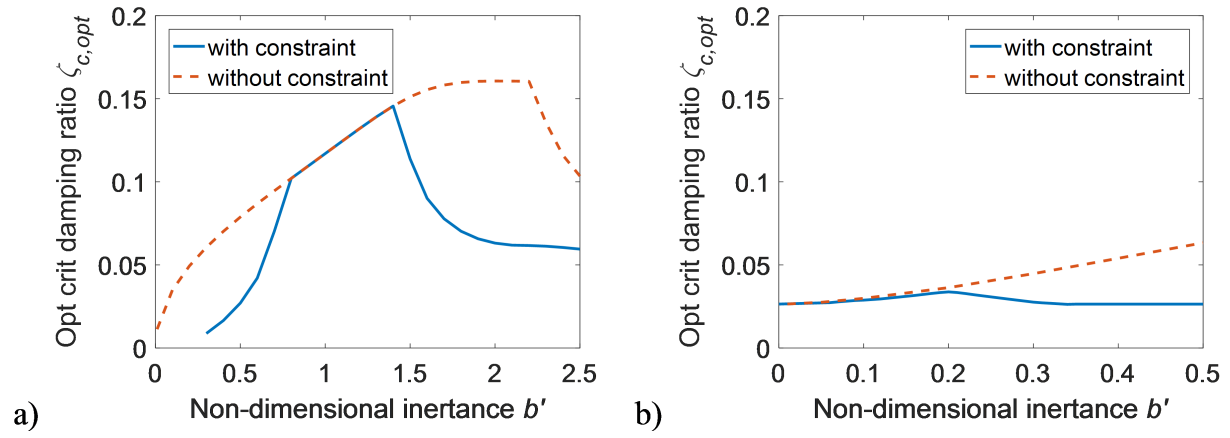


Fig. 12. Optimized damping ratio versus non-dimensional inertance with and without the constraint. (a) Layout III-4 and (b) Layout III-6, optimum critical damping ratio versus non-dimensional inertance

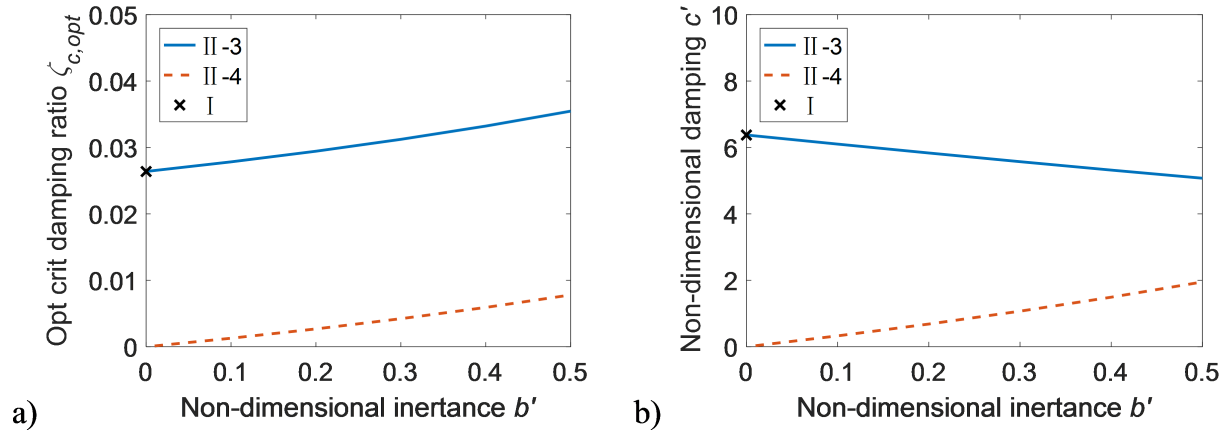


Fig. 13. Optimization results for beneficial layouts with one or two elements without the higher mode constraint. (a) Damping ratio and (b) corresponding non-dimensional damping coefficient, versus non-dimensional inertia

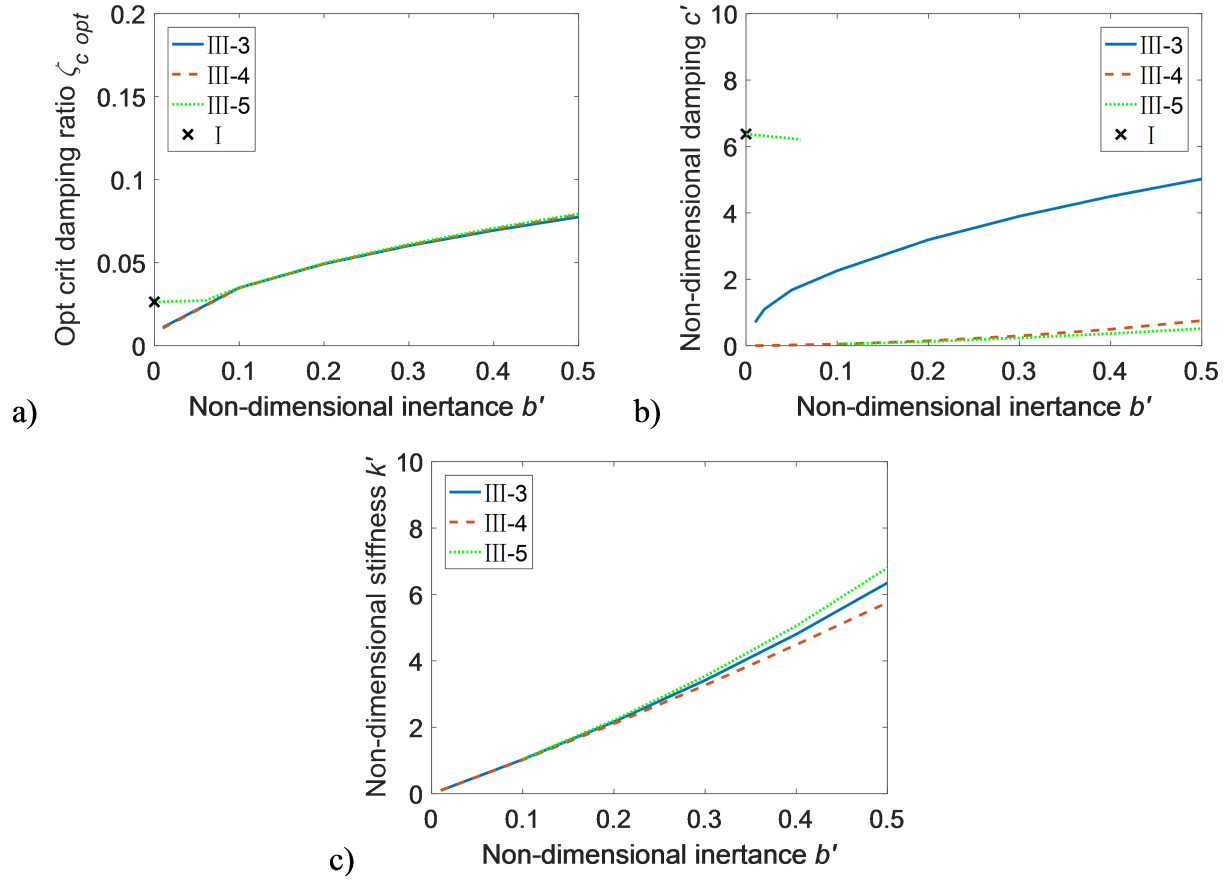


Fig. 14. Optimization results for beneficial layouts with three elements without the higher mode constraint. (a) Damping ratio, (b) corresponding non-dimensional damping coefficient and (c) corresponding non-dimensional frequency, versus non-dimensional inertia

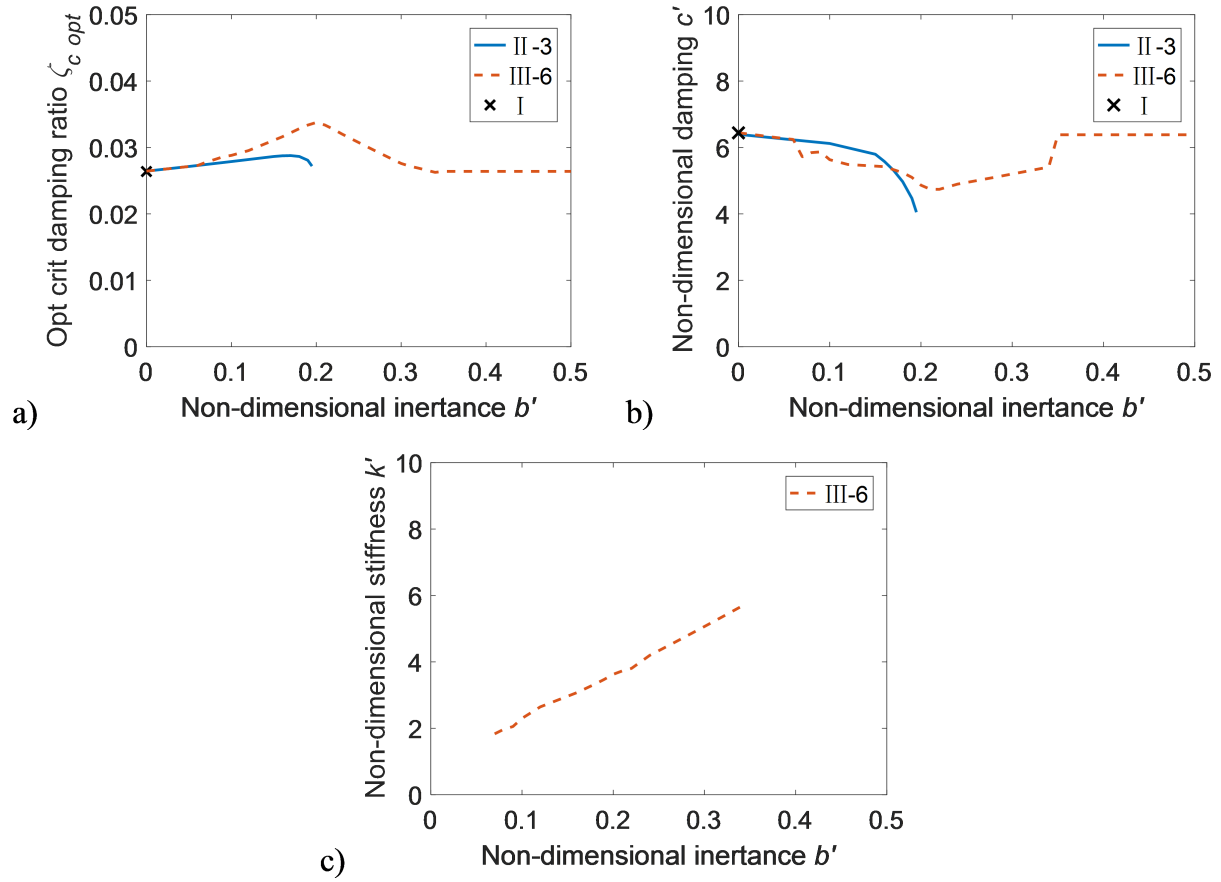


Fig. 15. Optimization results for beneficial layouts with the higher mode constraint. (a) Damping ratio, (b) corresponding non-dimensional damping coefficient and (c) corresponding non-dimensional frequency, versus non-dimensional inertia

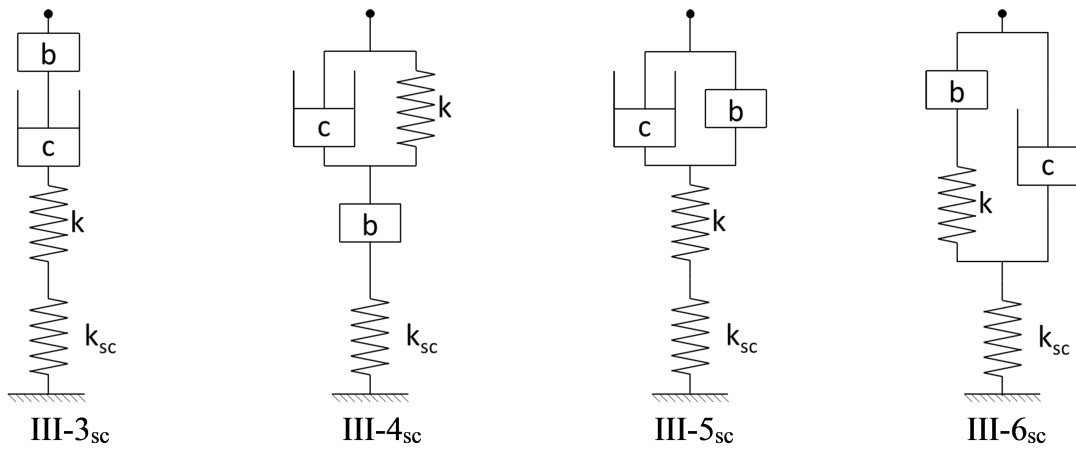


Fig. 16. Beneficial three-element layouts with added series compliance

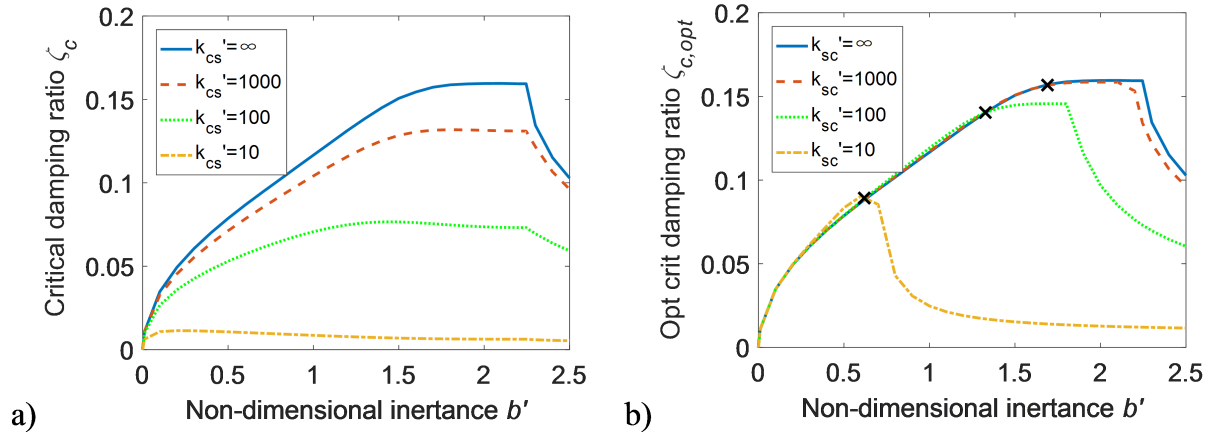


Fig. 17. Critical damping ratios with different series compliance (k'_{sc}) for Layout III-4_{sc} (a) with original optimized parameters (b) with re-optimized parameters

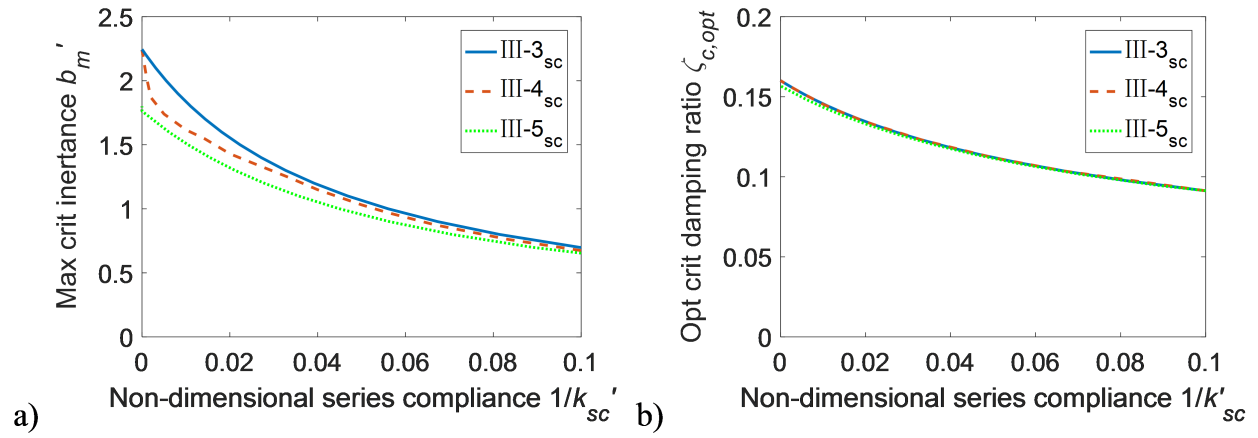


Fig. 18. Optimization results for Layouts III-3_{sc}, III-4_{sc} and III-5_{sc}. (a) Maximum critical inertance b'_m and (b) corresponding optimum critical damping ratio $\zeta_{c,opt}$, versus non-dimensional series compliance

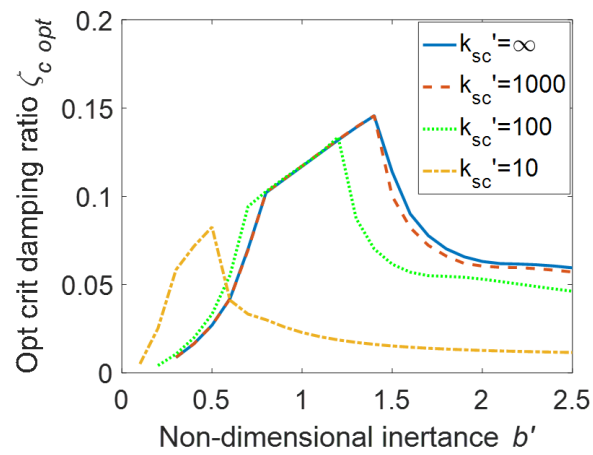


Fig. 19. Optimum critical damping ratio for Layout III-4_{sc}, versus non-dimensional inertance for re-optimized results with the constraint of higher mode and different series compliance